Hindawi
International Transactions on Electrical Energy Systems
Volume 2022, Article ID 7091937, 15 pages
https://doi.org/10.1155/2022/7091937

Research Article

Multi-Objective Optimal Power Flow including Wind and Solar Generation Uncertainty Using New Hybrid Evolutionary Algorithm with Efficient Constraint Handling Method

Ravi Kumar Avvari and Vinod Kumar D. M.

Department of Electrical Engineering, National Institute of Technology Warangal, Warangal, Telangana 506004, India

Correspondence should be addressed to Ravi Kumar Avvari; ravi22@student.nitw.ac.in

Received 10 February 2022; Revised 4 May 2022; Accepted 9 May 2022; Published 2 July 2022

Academic Editor: mahdiyeh eslami

A new hybrid decomposition-based multiobjective evolutionary algorithm is proposed for optimal power flow (OPF) including wind and solar generation uncertainty. This study recommends a novel constraint-handling method, which adaptively adds the penalty function and eliminates the parameter dependency on penalty function evaluation. The summation-based sorting and improved diversified selection methods are utilized to enhance the diversity of multiobjective optimization algorithms. The OPF problem is modeled as a multiobjective optimization problem with four objectives such as minimizing (i) total fuel cost (TC) including the cost of renewable energy source (RES), (ii) total emission (TE), (iii) active power loss (APL), and (iv) voltage magnitude deviation (VMD). The impact of RESs such as wind and solar energy sources on integration is considered in optimal power flow cost analysis. The costs of RESs are considered in the OPF problem to minimize the overall cost so that the impact of intermittence and uncertainty of renewable sources is studied in terms of cost and operation wise. The uncertainty of wind and solar energy sources is described using probability distribution functions (PDFs) such as Weibull and lognormal distributions. The efficiency of the algorithm is tested on IEEE 30-, IEEE 57-, and IEEE 118-bus systems for all possible conditions of renewable sources using Monte Carlo simulations.

1. Introduction

In recent times, RES penetration has drastically increased in the power system. The penetration of RESs has introduced many challenges to the power system. The intermittent nature of RESs makes the system more complex in terms of operation and control. The uncertain nature of RESs is required to be accurately modeled to examine the dynamic functioning of the power system. Due to its unpredictable nature, protection schemes need to be updated for operating the power system in a secure region. In a power system, the main aim is to operate it with optimal cost and simultaneously satisfy the operating and security constraints. The OPF determines the optimal control settings by the satisfying system and security constraints to economically operate.

A significant amount of research has been carried out in the domain of OPF with the incorporation of RESs in the power system using both deterministic and meta-heuristic optimization algorithms. The gradient method is proposed [1] to develop the dynamic OPF to include wind farms without considering the costs of wind power. For solving the OPF model in the presence of a wind plant, the authors [2] used the Newton method and interior-point methods. The uncertain nature of wind power has been estimated and is added to the overall cost function. However, deterministic methods are problem-specific, exhibit poor convergence characteristics, and are stuck at local optima points. Moreover, these methods are unable to solve real-world optimization issues. To overcome the drawbacks of deterministic methods, meta-heuristic methods have been introduced.

In [3], the authors used the SHADE algorithm with the SF method for arriving at the solution to OPF with RESs. Similarly, in [4–8] the authors proposed several metaheuristic optimization methods for solving OPF with RESs. However, these are formulated as single-objective optimization problems. In the real world, the OPF problem is multiobjective and the trade-off between multiple objects gives better optimal conditions for operation.

In [9], the authors introduced a modified JAYA algorithm for solving the MOOPF problem incorporating RESs with four different objectives. In this study, the authors transformed multiple objectives into a single objective problem with price and weights. Similarly, in [10–12] the authors proposed a weighted sum-based MOOPF problem with various objectives. The weighted sum-based methods are simple in combining multiobjectives into a single objective with suitable weights. However, this approach heavily depends on the weights that are assigned to each objective value, and these, in turn, affect the optimal solution. Moreover, the weighted sum-based methods fail to obtain the best-compromised solution when needed.

In [13], the authors concentrated on the analysis of the MOOPF solution with RESs using the hybrid DE and SOS algorithms, which have been tested under different operating conditions. Similarly, in [14–16] the authors used the nondominated sorting (NDS) technique to pick the best solutions for parents in an elitist fashion. When the dominant solutions are removed from the population, the effective exploration capability will be lost. Besides this, the nondominated sorting selection is challenging and time-consuming. Moreover, the constraints are handled using the penalty factor method, which is inefficient.

In OPF, constraints play a key role to obtain feasible optimal solutions. The constraint-handling techniques used in optimization techniques are divided into two categories; (i) generic methods and (ii) specific methods. The generic methods are penalty function-based methods. These are simple and mostly used in optimization algorithms as they do not demand additional changes in the algorithm. When a constraint violation occurs, a penalty is added to its fitness. However, these methods may not provide satisfactory results for all types of constraints. On the other hand, specific constraint-handling methods can be applied to convex region problems and large variable problems. The cutting plane method and gradient method are the commonly used methods to handle specific constraints [17, 18]. However, the drawback of specific methods is that, as the number of variables increases, the computing time also increases. The performance of both methods depends on fine-tuning different parameters of constraint handling, which also affects the fitness value.

The conventional generators are subjected to different costs as they run on fuel. RESs such as wind and solar do not require any fuel. Therefore, fuel costs are not considered for wind and solar power generation. In the case of wind and solar generations owned by anyone other than ISO, direct cost needs to be added to the total cost, which is in the form of maintenance costs and renewal charges [19]. The direct prices are agreed by ISO to pay for the scheduled wind and solar energy. Direct prices have not been addressed in most of the literature.

The above literature review reveals the following:

(i) Most of the authors designed the OPF problem as single-objective optimization. In real time, multiple objectives play a key role in the economic viability of the power system.

(ii) The weighted sum-based methods depend on weights assigned to each objective, and it affects the optimal solution.

(iii) In most of the literature, the Pareto dominance method is used, and in the Pareto dominance method, nondominated sorting (NDS) technique to select the best solutions is used, which improves the diversity and convergence. When all the dominant solutions have been removed, the diversity of the population is lost. NDS selection is complex and time-consuming.

(iv) The constraints are handled using the penalty factor method, a specific method that is inefficient, due to parameter dependency.

(v) In calculating the uncertainty cost of RESs, only overestimation and underestimation costs are considered, while the direct cost is neglected.

In this study, a new hybrid MOEA based on decomposition and summation of normalized objectives with an improved diversified selection method is used for the MOOPF problem. An SF strategy is employed to tackle various constraints (i.e., equality and inequality) of the MOOPF problem.

The major contributions of the research work include the following:

(1) Proposing a novel MOEA based on decomposition and summation of normalized objectives with improved diversified selection for the MOOPF problem.

(2) Integrating RESs like wind and solar power plants with conventional OPF to consider the impact of the uncertain nature of these sources.

(3) Modeling the uncertain nature of wind and solar power plants using PDF and calculating the uncertain cost using Monte Carlo simulations.

(4) Multiobjective OPF (MOOPF) with TC, TE, APL, and VMD as four objectives.

(5) Utilizing an efficient constraint-handling technique (CHT) called the superiority of feasible solution (SF) to tackle complex constraints in MOOPF problems.

The study is structured as follows: Section 2 presents a wind and solar uncertainty modeling. Section 3 describes the problem formulation of MOOPF with RES. Section 4 presents the framework of the proposed algorithm. In Section 5, simulation case studies are discussed and conclusions are made in Section 6.

2. Wind and Solar Power Uncertainty Modeling

The wind speed at a given geographical area is most likely distributed according to Weibull distributions. Mathematically, the Weibull PDF is written as follows:

$$f(v) = \left(\frac{k}{c}\right)\left(\frac{v}{c}\right)^{(k-1)}(e)^{(-v/c)^k}, \quad 0 < v < \infty. \tag{1}$$

The PDFs for two different shape and scale factors are given in [20]. The relationship between wind speed and power generation is as follows:

$$P_w(v) = \begin{cases} 0 & \text{for } v < v_{in} \text{ and } v > v_{out} \\ P_{wr}\left(\dfrac{v - v_{in}}{v_r - v_{in}}\right) & \text{for } v_{in} \le v_w \le v_r, \\ P_{wr} & \text{for } v_r < v_w \le v_{out} \end{cases} \tag{2}$$

The probability of obtaining a rated and zero power output is given by the following:

$$f_w(P_w = 0) = 1 - \exp\left(-\left(\frac{v_{in}}{c}\right)^k\right) + \exp\left(-\left(\frac{v_{out}}{c}\right)^k\right), \tag{3}$$

$$f_w(P_w = P_{wr}) = \exp\left(-\left(\frac{v_r}{c}\right)^k\right) + \exp\left(-\left(\frac{v_{out}}{c}\right)^k\right). \tag{4}$$

The probability for the linear part of the wind speed is given by the following:

$$f_w(P_w) = \left(\frac{k(v_r - v_{in})}{cP_{wr}}\right)\left(\frac{v_{in}P_{wr} + P_w(v_r - v_{in})}{cP_{wr}}\right)^{(k-1)} \cdot \exp\left(-\left(\frac{v_{in}P_{wr} + P_w(v_r - v_{in})}{cP_{wr}}\right)^k\right). \tag{5}$$

where Weibull PDF parameters k= 2 and $c = 10$. The wind speeds $v_{in} = 3$ m/sec, $v_{out} = 25$ m/sec, and $v_r = 16$ m/sec.

Similarly, the power output of a solar energy system is a factor of solar irradiance (G_s) and it likely follows the lognormal distribution [21]. The PDF for the lognormal distribution is as follows:

$$f_G(G_s) = \frac{1}{G_s\sigma\sqrt{2\pi}}\exp\left\{\frac{-(\ln G_s - \mu)^2}{2\sigma^2}\right\} \text{ for } G_s > 0. \tag{6}$$

The PV unit's solar irradiance to energy generation is [22]as follows:

$$P_s(G_s) = \begin{cases} P_{sr}\left(\dfrac{G_s^2}{G_{std}R_c}\right) \text{ for } 0 < G_s < R_c \\ P_{sr}\left(\dfrac{G_s}{G_{std}}\right) \text{ for } G_s \ge R_c \end{cases}, \tag{7}$$

where lognormal PDF parameters $\mu = 6$ and $\sigma = 0.6$. The standard solar irradiance (G_{std}) = 800 W/m^2, and particular irradiation point (R_c) = 120 W/m^2.

3. Problem Formulation with Renewable Energy Sources

In this study, a wind generator and solar generator are located at two different buses in the test system. Since wind and solar powers are intermittent, the Monte Carlo simulations are used to account for uncertainty and to calculate the uncertainty cost. The estimated price for the intermittency of wind and solar power is reflected in three ways: direct price, reserve price, and penalty price. Whenever power is underestimated, extra unusable power is wasted; however, in practical power system applications, such power can be saved in an energy storage system and thus counted as the reserve price. The price of overestimating power that is lower than the scheduled power is considered a penalty price in the case of overestimation.

3.1. Direct Price Calculation of Wind and Solar Power Plants. In contrast to conventional generators, wind and solar power generators do not require any fuel. When an ISO owns wind/PV facilities, the direct fuel cost may not occur except if the ISO intends to allocate any compensation for setting up or charging it as a renewal cost and repair work [22]. When private agencies own wind/PV plants, however, ISO proportionally pays for the agreed-upon scheduled power.

The direct price associated with j^{th} wind plants is as follows:

$$C_{w,j}\left(P_{ws,j}\right) = g_j P_{ws,j}. \tag{8}$$

Similarly, the direct price of k^{th} PV plant is as follows:

$$C_{s,k}\left(P_{ss,k}\right) = h_k P_{ss,k}. \tag{9}$$

3.2. Uncertainty Price Calculation of the Wind and Solar Power Plants. If the actual output power of the wind farm is lower than the predicted value, to ensure a constant supply of electricity to the consumers, the operator requires some spinning reserve. It is called the overestimation of power from unreliable sources. The cost incurred to maintain the spinning reserve is known as the reserve cost [23].

The reserve price of the j^{th} wind plant is as follows:

$$C_{Rw,j}\left(P_{ws,j} - P_{wav,j}\right) = K_{Rw,j}\left(P_{ws,j} - P_{wav,j}\right) = K_{Rw,j}\int_0^{Pws,j}\left(P_{ws,j} - p_{w,j}\right)f_w\left(p_{w,j}\right)dp_{w,j}. \tag{10}$$

In contrast to the overestimation scenario, when the actual power output of wind exceeds the predicted output, the surplus power generated by WT cannot be used and is wasted. This is called the underestimation of power from uncertain sources. In this case, ISO must pay a penalty for excess power.

The penalty price of the j^{th} wind plant is as follows:

$$C_{Pw,j}\left(P_{wav,j}-P_{ws,j}\right)=K_{Pw,j}\left(P_{wav,j}-P_{ws,j}\right)=K_{Pw,j}\int_{P_{ws,j}}^{P_{wr,j}}\left(p_{w,j}-P_{ws,j}\right)f_w\left(p_{w,j}\right)dp_{w,j}. \tag{11}$$

In the same way as the wind plant, the PV plant also has intermittency in power output. The reserve and penalty price equations for PV plants are described as follows [24].

Reserve price for k^{th} PV plant is as follows:

$$C_{Rs,k}\left(P_{ss,k}-P_{sav,k}\right)=K_{Rs,k}\left(P_{ss,k}-P_{sav,k}\right)=K_{Rs,k}*f_s\left(P_{sav,k}<P_{ss,k}\right)*\left[P_{ss,k}-E\left(P_{sav,k}<P_{ss,k}\right)\right]. \tag{12}$$

The penalty price for a k^{th} PV plant is as follows:

$$C_{Ps,k}\left(P_{sav,k}-P_{ss,k}\right)=K_{Ps,k}\left(P_{sav,k}-P_{ss,k}\right)=K_{Ps,k}*f_s\left(P_{sav,k}>P_{ss,k}\right)*\left[E\left(P_{sav,k}>P_{ss,k}\right)-P_{ss,k}\right], \tag{13}$$

where the direct, penalty, and reserve price coefficients of wind and PV plants are 1.6, 1.5, and 3, respectively.

3.3. Objective Functions. The MOOPF problem assumed the minimization of four objectives: (i) TC, (ii) TE, (iii) APL, and (iv) VMD. The objectives can be described as follows:

$$f_{TC}=\sum_{i=1}^{N_{TG}}a_i+b_iP_{TGi}+c_iP_{TGi}^2+\sum_{j=1}^{N_{WG}}\left[C_{w,j}\left(P_{ws,j}\right)+C_{Rw,j}\left(P_{ws,j}-P_{wav,j}\right)+C_{Pw,j}\left(P_{wav,j}-P_{ws,j}\right)\right]+\sum_{k=1}^{N_{SG}}\left[C_{s,k}\left(P_{ss,k}\right)+C_{Rs,k}\left(P_{ss,k}-P_{sav,k}\right)+C_{Ps,k}\left(P_{sav,k}-P_{ss,k}\right)\right], \tag{14}$$

$$f_{TE}=\sum_{i=1}^{N_{TG}}\left(\alpha_i+\beta_iP_{TGi}+\gamma_iP_{TGi}^2+\xi_ie^{\lambda_iP_{TGi}}\right), \tag{15}$$

$$f_{APL}=\sum_{k=1}^{N_L}\left(G_k\left(V_i^2+V_j^2-2V_iV_j\cos\theta_{ij}\right)\right), \tag{16}$$

$$f_{VMD}=\sum_{i=1}^{N_{PQ}}\left|\left(V_i-V_{ref}\right)\right|, \tag{17}$$

where V_{ref} = 1.0 p.u., i.e., reference voltage.

3.4. Constraints

3.4.1. Equality Constraints. The overall demand and losses throughout the system are equal to the total real and reactive power delivered.

$$P_{G_i}-P_{D_i}-V_i\sum_{j=1}^{N_B}V_j\left[G_{ij}\cos\theta_{ij}+B_{ij}\sin\theta_{ij}\right]=0::\forall i\in N_B, \tag{18}$$

$$Q_{G_i}-Q_{D_i}-V_i\sum_{j=1}^{N_B}V_j\left[G_{ij}\sin\theta_{ij}-B_{ij}\cos\theta_{ij}\right]=0::\forall i\in N_B. \tag{19}$$

3.4.2. Inequality Constraints. Generator constraints

$$P_{TGi}^{\min}\le P_{TGi}\le P_{TGi}^{\max};\forall i\in N_{TG}, \tag{20}$$

$$P_{WGi}^{\min}\le P_{WGi}\le P_{WGi}^{\max};\forall i\in N_{WG}, \tag{21}$$

$$P_{SGi}^{\min}\le P_{SGi}\le P_{SGi}^{\max};\forall i\in N_{SG}, \tag{22}$$

$$Q_{TGi}^{\min}\le Q_{TGi}\le Q_{TGi}^{\max};\forall i\in N_{TG}, \tag{23}$$

$$Q_{WGi}^{\min}\le Q_{WGi}\le Q_{WGi}^{\max};\forall i\in N_{WG}, \tag{24}$$

$$Q_{SGi}^{\min}\le Q_{SGi}\le Q_{SGi}^{\max};\forall i\in N_{SG}, \tag{25}$$

$$V_{Gi}^{\min}\le V_{Gi}\le V_{Gi}^{\max};\forall i\in N_G. \tag{26}$$

Transformer constraints

$$T_k^{\min} \le T_k \le T_k^{\max}; \forall k \in N_T. \quad (27)$$

Shunt VAR compensator constraints

$$Q_{ci}^{\min} \le Q_{ci} \le Q_{ci}^{\max}; \forall i \in N_C. \quad (28)$$

Security constraints

$$V_{Lp}^{\min} \le V_{Lp} \le V_{Lp}^{\max}; \forall p \in N_L, \quad (29)$$

$$S_{lq} \le S_{lq}^{\max}; \forall q \in n_l. \quad (30)$$

Two equality constraints (equations (18) and (19)) are automatically satisfied when the power flow converges to an optimal solution. The generator buses' real power (excluding slack bus), transformer tap ratios, voltage limits, and shunt compensator ranges are considered as control variables that are self-limiting. The remaining inequality constraints require constraint-handling techniques.

In OPF, generator reactive power capacities are significant. In the case of thermal generators, the ranges are considered as in [25, 26]. In recent years, WTs with complete reactive power capability have become commercially viable [27]. Enercon FACTS-WT can deliver reactive power in the range of -0.4p.u.to 0.5p.u. The negative sign signifies the generator's ability to absorb. Rooftop solar PV is designed as load buses with zero reactive power. However, because utility-based solar PVs have converters built-in, full generator modeling is required due to the converters' dynamic behavior [28]. In this study, the reactive power capabilities of solar PV are assessed between −0.4p.u and 0.5p.u.

3.5. Superiority of Feasible Solution (SF) Method. The most commonly used constraint-handling technique is the penalty function method. When a constraint violation occurs, its solution is penalized. Owing to its simplicity and ease of operation, the outcome of this method is strongly contingent on the penalty factor, which is to be chosen using trial and error, going to cause the fitness value to deteriorate. This study deployed a new CHT called the SF technique [29], which does not require any penalty coefficient.

Since MOOPF is a constrained optimization problem, it requires a better-constrained handling method. In this study, the SF technique [29] was employed to solve the MOOPF problem with RESs. The steps followed when comparing two solutions are as follows:

(1) While comparing two nonfeasible solutions, the solution having the smallest constraint violation is selected.

(2) When two feasible solutions are compared, the one with a better fitness solution is selected.

(3) When a feasible solution is compared to a nonfeasible solution, the feasible solution is selected.

By incorporating these three rules into the proposed algorithm to solve the MOOPF problem, two situations arise, the first of which is when the population size is lower than the number of feasible solutions, and the second method is to ignore nonfeasible solutions. The use of the summation-based method is to select feasible solutions if the number of feasible solutions is greater than the population size.

4. Proposed Algorithm

The MOEAs are normally modeled to handle different conflicting goals, such as maximizing the spread of solutions along the Pareto front (i.e., diversity) and minimizing the distance between the solutions along the Pareto front (i.e., convergence) [30]. The trade-off between convergence and diversity is important to choose the best solution among the obtained solutions. Therefore, to attain a balance between exploration and exploitation in this study, a new method is proposed.

In this study, a summation of normalized objective values (SNOVs) with improved diversified selection (IDS) is proposed and integrated with the multiobjective evolution algorithm based on the decomposition (MOEA/D) [31] method to solve the MOOPF problem with RES. The MOEA/D method decomposes the multiobjective optimization problem into several single scalar optimization problems and optimizes them all at the same time using weight vectors. The weight vectors' distance is used to create neighborhoods. In every population evolution, information from the neighborhood is used to find a solution. The nondominated sorting used in MOEA/D is complex and time-consuming. Some useful information may be lost if the dominant solutions are completely discarded. In addition, diversity may be lost during the search process and lead to local optima. To overcome these problems, the summation of normalized objective values with IDS [32] is employed in this study instead of nondominated sorting selection to get uniformly distributed Pareto front and improved convergence characteristics.

A new constraint-handling strategy called the superiority of feasible solution (SF) method is employed to handle the various constraints (i.e., equality and inequality) of the MOOPF problem. The proposed algorithm utilizes the fuzzy method to get the best-compromised values. The outcomes of the proposed method are compared with popular methods like MOEA/D [33], NSGA-II [34], and MOPSO [35] for different cases.

The pseudocode of the proposed method is as follows:

Step 1. **Initialization:** Generate the initial population (P_t) of size N. Using SSA [36], generate uniformly distributed weights, and the number of weight vectors is defined as follows:

$$N(D, M) = \begin{pmatrix} D + M - 1 \\ M - 1 \end{pmatrix} \text{for } D > 0. \quad (31)$$

Step 2. Run the load flow and evaluate the fitness values of the selected objective functions and total constraint violations.

Step 3. Using angle criteria [37], locate neighbors with the smallest angles for each weight vector. The following is an example of the angle criteria:

$$\tan\theta = \frac{d_2}{d_1}, \tag{32}$$

where $d_1 = (\|w_i^T w_j\|/\|w_j\|)$, $d_2 = \|w_i - d_1(w_j/\|w_j\|)\|$, $i, j = 1, 2, \ldots, N$, and $i \neq j$, θ = angle between d_1 and d_2.

Step 4. Evaluate the smaller objective values to form the present ideal point.

Step 5. Evaluate the larger objective values to form the present nadir point.

Step 6. **Reproduction:** Angle criteria are used to choose N pairs of mating parents. A set of mating parents is picked with a probability of δ each weight.

Step 7. To generate the new population (Q_t), use two-point crossover and mutation.

Step 8. The new population is formed by combining the original population (P_t) with the newly generated population (Q_t).

Step 9. For each objective and solution, calculate the normalized objective values.

Step 10. By adding all of the normalized objective values for each solution, obtain the sum of the normalized objective values [32].

For $m = 1$ to M,

Calculate the max and min objectives of *the* m^{th} objective and find its range.

Normalize the m^{th} objective values using the expression:

$$f'_m(x) = \frac{f_m(x) - f_{\min}}{f_{\max} - f_{\min}}. \tag{33}$$

End.

For $i = 1$ to N.

Add up all normalized objectives to get a unique value.

End.

Step 11. Calculate the Euclidean space between all of the solutions and the reference point.

Step 12. Set a stopping point for the individual with the shortest path to the original point.

Step 13. Divide the objective range into 100 bins, and scan all bins till you reach the stopping point. The solution having the least summation value will be picked to enter into the preferential set for each scanned bin.

Table 1: Various case studies considered in this study.

Case name	Test system	TC	TE	APL	VMD
Case-1	IEEE 30-bus	✓	✓	—	—
Case-2		✓	—	✓	—
Case-3		✓	✓	✓	—
Case-4		✓	✓	—	✓
Case-5		✓	✓	✓	✓
Case-6	IEEE 57-bus	✓	✓	—	—
Case-7		✓	✓	✓	—
Case-8		✓	✓	✓	✓
Case-9	IEEE 118-bus	✓	—	✓	—
Case-10		✓	—	✓	✓

Step 14. The solutions are dominated by stopping points, and also the individuals who were not selected will be sent to the backup set.

Step 15. Apply the fuzzy min-max method [38] to get the best-compromised values.

5. Simulation Results

In this study, to tackle the MOOPF problem including wind and photovoltaic uncertainties, the proposed method, MOEA/D [33], NSGA-II [34], and MOPSO [35] are demonstrated on IEEE 30-, IEEE 57-, and IEEE 118-bus power systems. It is implemented in MATLAB R2016a and runs on an i3 processor with 4 GB RAM.

In general, more than two objectives are treated as a multiobjective optimization (MOO) problem. While formulating the MOO problem, the objectives are chosen such that the objectives conflict with each other. The conflict between objectives depends on the correlation among the objectives. Different objectives will have different degrees of correlation among the combination of objectives. To formulate the combination of objectives, four different objective functions are considered, which are as follows: (i) TC, (ii) TE, (iii) APL, and (iv) VMD. A total of ten different case studies are considered on three standard test systems to test the efficiency of the proposed method for the MOOPF problem. The various case studies considered in this study are given in Table 1.

Numerous trials with various control parameters were conducted, and the best findings obtained are summarized in this study. The parameters chosen for each method are listed in Table 2.

5.1. Modified IEEE 30-Bus System. The IEEE 30-bus power system has 6 thermal generators placed at buses 1, 2, 5, 8, 11, and 13 (# 1 generator as a slack generator), 41 lines. In this study, 4 off-nominal transformers are considered between lines 6–10, 6–9, 4–12, and 27–28, and 9 shunt VAR compensators are placed at the buses. The whole real and reactive power demand on the system is 238.40 MW and 126.20MVAR, respectively. In addition to the above thermal generators, one wind generator and one solar generator are added to buses 22 and 25, respectively. Detailed information about the test system is provided in [39, 40].

Table 2: Control parameters used in different methods.

S. No.	Method	Control parameters
1.	Proposed method	Population size (N) = 100, number of divisions made along with every object (D) = 12, neighborhood size (T) = 20, crossover probability (P_c) = 1.0, mutation probability (P_m) = 0.05, and number of iterations = 100.
2.	MOEA/D [33]	Population size (N) = 100, number of divisions made along with every object (D) = 12, neighborhood size (T) = 20, crossover probability (P_c) = 1.0, mutation probability (P_m) = 0.05, and number of iterations = 100.
3.	NSGA-II [34]	Population size (N) = 100, crossover probability (P_c) = 0.8, No. of iterations = 100, and mutation probability (P_m) = 0.01.
4.	MOPSO [35]	Population size (N) = 100, $C1 = C2 = 2$, $W = 0.5$, and number of iterations = 100.

Table 3: IEEE 30-bus system: best-compromised values obtained by the proposed method for Case-1 to Case-5.

S. no.	Control variables	Control variables at bus/line	Limits		Case-1	Case-2	Case-3	Case-4	Case-5
			Min	Max					
1.	Power (MW)	2	20	80	49.3631	43.5939	49.7998	49.9396	49.9289
2.		5	15	50	26.7537	30.5688	36.3853	25.7456	41.2671
3.		8	10	35	27.5324	27.0078	30.5428	24.1533	29.4956
4.		11	10	30	18.8816	20.4392	25.7521	22.0017	21.0325
5.		13	12	40	23.9297	21.8609	27.6149	23.8890	27.9709
6.		22	0	50	31.2931	33.0888	29.7074	32.1679	32.2785
7.		25	0	50	35.4439	29.3993	31.1763	33.7683	28.2922
8.	Voltage (p.u)	1	0.95	1.1	1.0427	1.0496	1.0476	1.0301	1.0212
9.		2	0.95	1.1	1.0354	1.0392	1.0387	1.0245	1.0147
10.		5	0.95	1.1	1.0008	1.0131	1.0174	1.0154	1.0011
11.		8	0.95	1.1	1.0113	1.0285	1.0346	0.9869	0.9972
12.		11	0.95	1.1	1.0126	1.0260	1.0020	1.0104	1.0070
13.		13	0.95	1.1	1.0297	1.0171	1.0148	1.0165	1.0098
14.		22	0.95	1.1	1.0303	1.0256	1.0174	1.0030	1.0067
15.		25	0.95	1.1	1.0386	1.0422	1.0267	1.0190	1.0212
16.	Tap ratio	11	0.9	1.1	1.0144	1.0257	0.9974	1.0143	1.0220
17.		12	0.9	1.1	1.0319	1.0350	1.0238	1.0051	0.9908
18.		15	0.9	1.1	1.0044	0.9896	0.9943	0.9677	0.9719
19.		36	0.9	1.1	0.9880	0.9955	1.0249	0.9660	0.9721
20.	Shunt VAR compensator (MVAR)	10	0	5	3.1425	1.9772	2.0710	3.0865	2.7684
21.		12	0.	5	1.9108	2.5250	3.7790	1.9405	1.6628
22.		15	0	5	1.8903	2.5177	2.1385	2.9160	3.9393
23.		17	0	5	2.4423	2.9065	3.1406	2.9999	2.5418
24.		20	0	5	2.2654	2.7249	2.4215	3.6789	2.9067
25.		21	0	5	2.3629	1.3956	2.2982	2.1017	1.7645
26.		23	0	5	2.9082	2.7610	2.8149	1.9246	1.6307
27.		24	0	5	2.3035	2.9588	2.2973	1.9558	3.3332
28.		29	0	5	2.7370	2.6593	2.4329	2.9911	2.3346
1.	TC ($/h)	-	-	-	794.0907	798.6845	838.0936	799.7882	851.9069
2	TE (ton/h)	-	-	-	0.2166	-	0.2049	0.2172	0.2057
3.	APL (MW)	-	-	-	-	3.9899	3.2506	-	3.1972
4.	VMD (p.u.)	-	-	-	-	-	-	0.0902	0.1038

5.1.1. Case-1: Simultaneously Minimize TC and TE. In this case, TC and TE are the objectives considered to simultaneously minimize. The optimal decision variables obtained by the suggested method are included in Table 3. The best-compromised values that could be found using the proposed algorithm have a TC of **794.0907$/h** and a TE of **0.2166ton/h,** which is the lowest value compared with MOEA/D [33], NSGA-II [34], and MOPSO [35] as shown in Table 4. The Pareto optimal fronts of all the methods are depicted in Figure 1.

5.1.2. Case-2: Simultaneously Minimize TC and APL. In this case, TC and APL are the objectives considered to simultaneously minimize. The optimal decision variables obtained by the suggested method are included in Table 3. The best-compromised values that could be found using the proposed algorithm have a TC of **798.6845$/h** and an APL of **3.9899 MW,** which is the lowest value compared with MOEA/D [33], NSGA-II [34], and MOPSO [35] as shown in Table 4. The Pareto optimal fronts of all the methods are depicted in Figure 2.

Table 4: IEEE 30-bus system: comparison of the proposed method with MOEA/D [33], NSGA-II [34], and MOPSO [35] for Case-1 to Case-5.

Case name	Objective functions	Proposed method	MOEA/D [33]	NSGA-II [34]	MOPSO [35]
Case-1	TC ($/h)	**794.0907**	794.2012	794.4894	794.1736
	TE (ton/h)	**0.2166**	0.2170	0.2171	0.2203
Case-2	TC ($/h)	**798.6845**	798.9000	805.4298	816.1819
	APL (MW)	**3.9899**	4.0790	4.0319	4.2422
Case-3	TC ($/h)	**838.0936**	840.0000	848.6240	870.9164
	TE (ton/h)	**0.2048**	0.2043	0.2062	0.2198
	APL (MW)	**3.2506**	3.7170	3.3119	4.1321
Case-4	TC ($/h)	**799.7880**	801.7412	800.9397	831.3916
	TE (ton/h)	**0.2172**	0.2164	0.2173	0.2386
	VMD (p.u.)	**0.0902**	0.1271	0.1229	0.1434
Case-5	TC ($/h)	**851.9069**	855.4589	858.7833	862.8927
	TE (ton/h)	**0.2057**	0.2101	0.2137	0.2540
	APL (MW)	**3.1972**	3.1997	3.2025	3.4352
	VMD (p.u.)	**0.1038**	0.1912	0.2635	0.4925

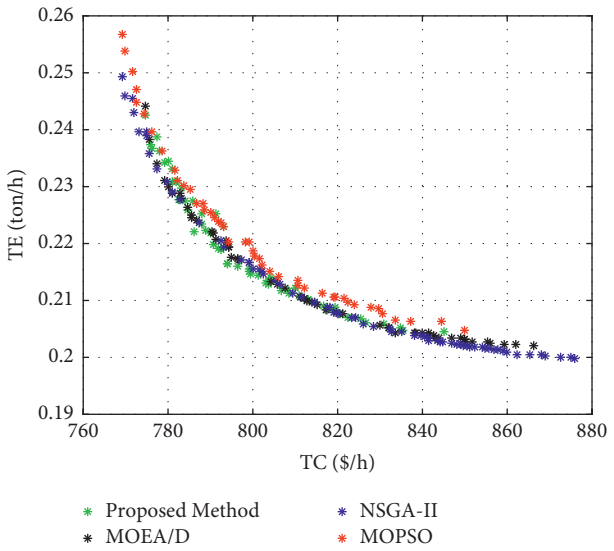

Figure 1: Case-1: IEEE 30-bus system Pareto optimal fronts.

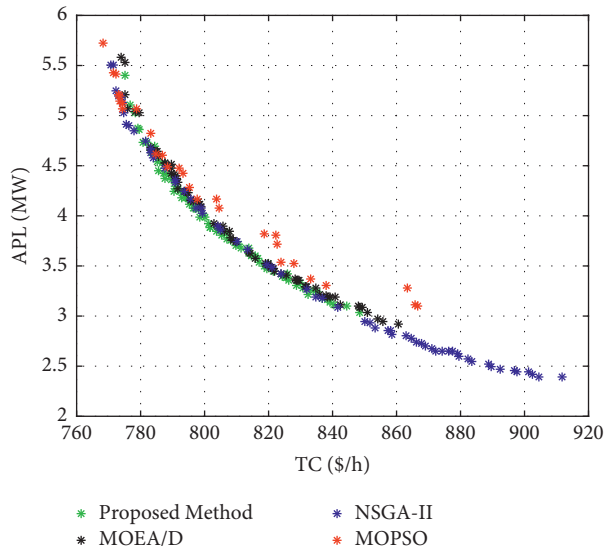

Figure 2: Case-2: IEEE 30-bus system Pareto optimal fronts.

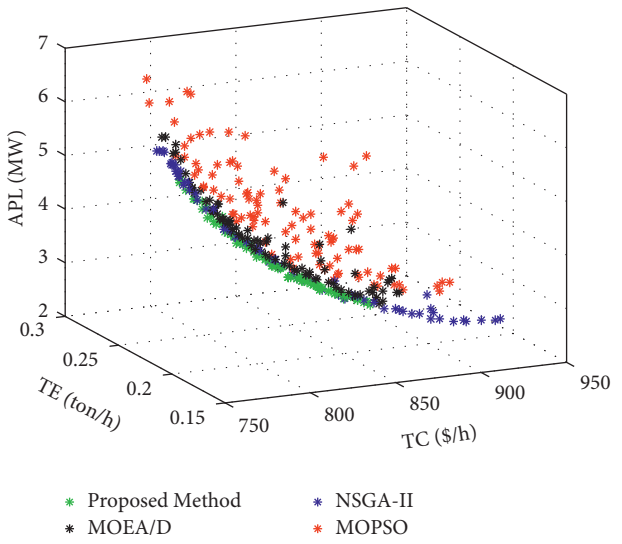

Figure 3: Case-3: IEEE 30-bus system Pareto optimal fronts.

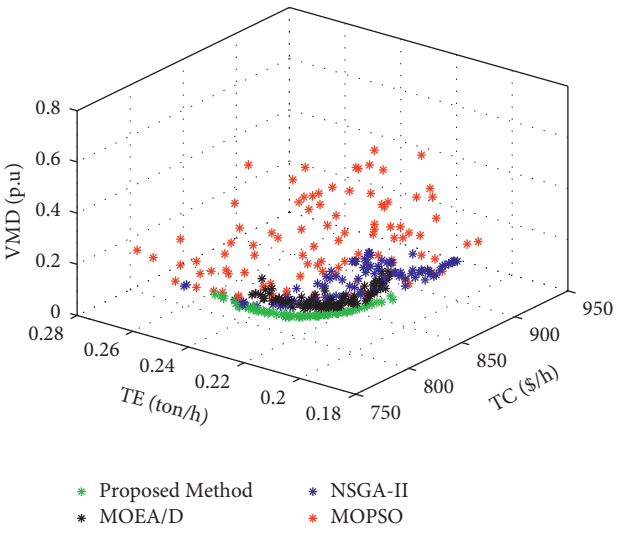

Figure 4: Case-4: IEEE 30-bus system Pareto optimal fronts.

Table 5: IEEE 57-bus system: best-compromised values obtained by the proposed method for Case-6 to Case-8.

S. no.	Control variables	Control variables at bus/line	Limits		Case-6	Case-7	Case-8
			Min	Max			
1.	Power (MW)	2	0	100	98.1298	67.1046	74.8586
2.		3	0	140	69.4063	55.0118	64.1958
3.		6	0	100	70.9842	98.4255	52.0615
4.		8	0	550	329.0458	306.7587	315.7318
5.		9	0	100	72.7441	99.3728	98.8024
6.		12	0	410	315.2646	341.6928	378.7730
7.		45	0	80	79.6017	79.9551	79.8243
8.		46	0	80	79.8919	79.9311	79.5757
9.	Voltage (p.u.)	1	0.95	1.1	1.0481	1.0296	1.0391
10.		2	0.95	1.1	1.0371	1.0246	1.0333
11.		3	0.95	1.1	1.0340	1.0227	1.0229
12.		6	0.95	1.1	1.0275	1.0185	1.0209
13.		8	0.95	1.1	1.0295	1.0162	1.0318
14.		9	0.95	1.1	1.0169	1.0099	1.0160
15.		12	0.95	1.1	1.0369	1.0268	1.0217
16.		45	0.95	1.1	1.0471	1.0498	1.0514
17.		46	0.95	1.1	1.0209	1.0372	1.0175
18.	Tap ratio	19	0.9	1.1	1.0154	1.0139	1.0056
19.		20	0.9	1.1	0.9945	1.0497	1.0367
20.		31	0.9	1.1	1.0183	1.0260	0.9955
21.		35	0.9	1.1	0.9938	1.0263	0.9876
22.		36	0.9	1.1	0.9601	0.9982	0.9821
23.		37	0.9	1.1	0.9943	1.0176	1.0321
24.		41	0.9	1.1	1.0225	0.9911	1.0155
25.		46	0.9	1.1	0.9889	0.9757	0.9456
26.		54	0.9	1.1	0.9999	0.9233	0.9049
27.		58	0.9	1.1	0.9814	0.9802	0.9613
28.		59	0.9	1.1	1.0108	0.9877	1.0070
29.		65	0.9	1.1	0.9914	0.9841	0.9967
30.		66	0.9	1.1	0.9748	0.9484	0.9140
31.		71	0.9	1.1	0.9703	0.9756	0.9547
32.		73	0.9	1.1	1.0158	0.9829	1.0058
33.		76	0.9	1.1	0.9691	0.9769	0.9649
34.		80	0.9	1.1	0.9908	0.9872	1.0199
35.	Shunt VAR compensator (MVAR)	18	0	20	9.1150	11.4035	11.0379
36.		25	0	20	9.8438	10.4059	8.2934
37.		53	0	20	11.2830	7.1925	7.7894
1.	TC ($/h)	-	-	-	36195.21	36096.69	36207.21
2.	TE (ton/h)	-	-	-	1.0182	1.0238	1.1383
3.	APL (MW)	-	-	-	-	10.3303	9.9732
4.	VMD (p.u.)	-	-	-	-	-	0.6848

5.1.3. Case-3: Simultaneously Minimize TC, TE, and APL. In this case, TC, TE, and APL are the objectives considered to simultaneously minimize. The optimal decision variables obtained by the suggested method are included in Table 3. The best-compromised values that could be found using the proposed algorithm have a TC of **838.0936 $/h**, a TE of **0.2049ton/h,** and an APL of **3.2506 MW,** which is the lowest value compared with MOEA/D [33], NSGA-II [34], and MOPSO [35] as shown in Table 4. The Pareto optimal fronts of all the methods are depicted in Figure 3.

5.1.4. Case-4: Simultaneously Minimize TC, TE, and VMD. In this case, TC, TE, and VMD are the objectives considered to simultaneously minimize. The optimal decision variables obtained by the suggested method are included in Table 3. The best-compromised values that could be found using the proposed algorithm have a TC of **799.7880$/h**, a TE of **0.2172ton/h,** and a VMD of **0.0902p.u.,** which is the lowest value compared with MOEA/D [33], NSGA-II [34], and MOPSO [35] as shown in Table 4. The Pareto optimal fronts of all the methods are depicted in Figure 4.

5.1.5. Case-5: Simultaneously Minimize TC, TE, APL, and VMD. In this case, TC, TE, APL, and VMD are the objectives considered to be simultaneously minimized. The optimal decision variables obtained by the suggested method are included in Table 3. The best-compromised values that could be found using the proposed algorithm have a TC of

Table 6: IEEE 57-bus system: comparison of the proposed method with MOEA/D [33], NSGA-II [34], and MOPSO [35] for Case-6 to Case-8.

Case name	Objective functions	Proposed method	MOEA/D [33]	NSGA-II [34]	MOPSO [35]
Case-6	TC ($/h)	**36195.21**	36198.87	36399.10	36733.34
	TE (ton/h)	**1.0182**	1.0271	1.0912	1.1145
Case-7	TC ($/h)	**36096.69**	36990.02	36363.70	39208.74
	TE (ton/h)	**1.0238**	1.0782	1.1288	1.0890
	APL (MW)	**10.3303**	10.7016	10.7953	11.0434
Case-8	TC ($/h)	**36207.21**	36317.56	36479.38	37321.91
	TE (ton/h)	**1.0916**	1.1256	1.1382	1.2049
	APL (MW)	**9.9732**	11.2487	11.3923	14.5232
	VMD (p.u.)	**0.6848**	0.6954	0.8907	0.8323

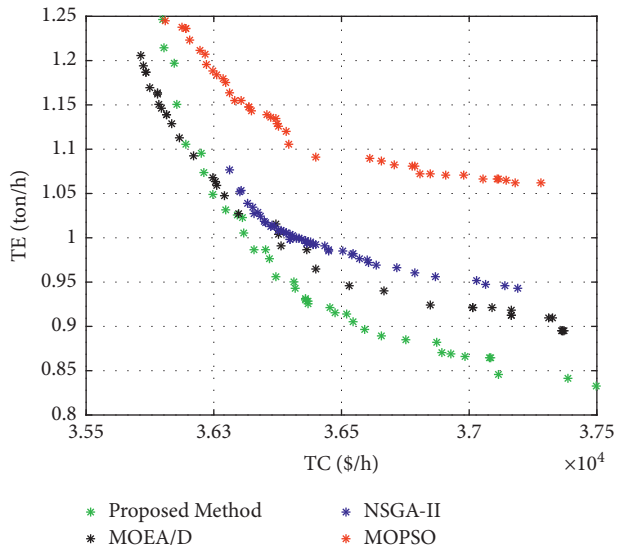

Figure 5: Case-6: IEEE 57-bus system Pareto optimal fronts.

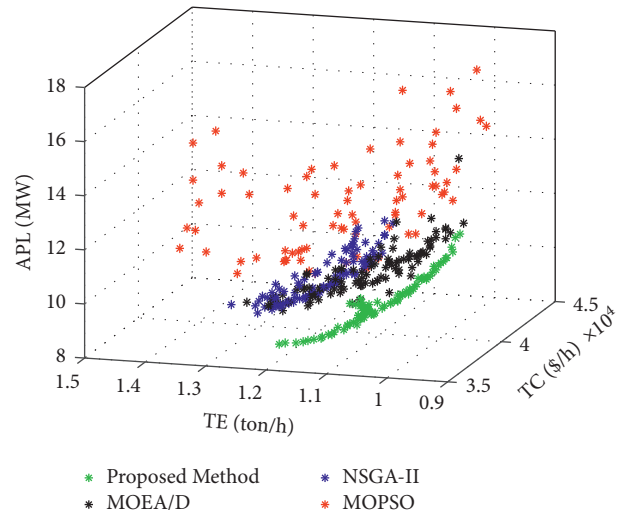

Figure 6: Case-7: IEEE 57-bus system Pareto optimal fronts.

851.9069$/h, a TE of **0.2057ton/h,** APL of **3.1972 MW**, and VMD of **0.1038p.u.,** which is the lowest value compared with MOEA/D [33], NSGA-II [34], and MOPSO [35] as shown in Table 4.

5.2. Modified IEEE 57-Bus System. To show the scalability of the proposed algorithm, the IEEE 57-bus system is used for solving the MOOPF problem. It contains 7 thermal generators placed at buses 1, 2, 3, 6, 8, 9, and 12 (# 1 generator as a slack generator), 80 lines. In this study, 15 off-nominal transformers are considered along with 3 shunt VAR compensators. The entire real and reactive power demand on the system is 1250.80 MW and 336.40MVAR, respectively. In addition to the above thermal generators, one wind generator and one solar unit are added at buses 45 and 46, respectively. Detailed information about the test system is provided in [39, 40].

5.2.1. Case-6: Simultaneously Minimize TC and TE. In this case, TC and TE are the objectives that need to be simultaneously minimized. The optimal decision variables obtained by the suggested method are included in Table 5. The best compromise solution that could be found using the proposed algorithm has a TC of **36195.21$/h** and a TE of **1.0182ton/h,** which is the lowest value compared with MOEA/D [33], NSGA-II [34], and MOPSO [35] as shown in Table 6. The Pareto optimal fronts of all the methods are depicted in Figure 5.

5.2.2. Case-7: Simultaneously Minimize TC, TE, and APL. In this case, TC, TE, and APL are the objectives that need simultaneous minimizing. The optimal decision variables obtained by the suggested method are included in Table 5. The best-compromised values that could be found using the proposed algorithm have a TC of **36096.69$/h**, a TE of **1.0238ton/h,** and an APL of **10.3303 MW,** which is the lowest value compared with MOEA/D [33], NSGA-II [34], and MOPSO [35] as shown in Table 6. The Pareto optimal fronts of all the methods are depicted in Figure 6.

5.2.3. Case-8: Simultaneously Minimize TC, TE, APL, and VMD. In this case, TC, TE, APL, and VMD are the objectives that need to be simultaneously minimized. The optimal decision variables obtained by the suggested method are included in Table 5. The best-compromised values that

Table 7: IEEE 118-bus system: best-compromised values obtained by the proposed method for Case-9 to Case-10.

Variables	Bus/line	Limits		Case-9	Case-10	Variables	Bus/line	Limits		Case-9	Case-10
		min	max					min	max		
	1	0	100	31.118	52.020		31	0.95	1.1	1.0253	1.0169
	4	0	100	21.400	41.520		32	0.95	1.1	1.0195	1.0030
	6	0	100	42.530	40.834		34	0.95	1.1	0.9909	1.0094
	8	0	100	28.556	26.448		36	0.95	1.1	1.0241	1.0067
	10	0	550	273.35	245.999		40	0.95	1.1	1.0096	1.0118
	12	0	185	86.663	95.235		42	0.95	1.1	1.0305	1.0113
	15	0	100	43.268	37.779		46	0.95	1.1	1.0150	1.0221
	18	0	100	99.997	45.659		49	0.95	1.1	1.0118	1.0055
	19	0	100	35.781	55.328		54	0.95	1.1	1.0359	1.0023
	24	0	100	64.585	35.747		55	0.95	1.1	1.0708	1.0239
	25	0	320	182.60	90.928		56	0.95	1.1	1.0661	1.0256
	26	0	414	0.000	162.842		59	0.95	1.1	1.0619	1.0271
	27	0	100	24.090	46.656		61	0.95	1.1	1.1000	1.0175
	31	0	107	22.783	25.781		62	0.95	1.1	1.0982	0.9985
	32	0	100	62.386	37.325		65	0.95	1.1	1.0875	1.0049
	34	0	100	43.187	40.202		66	0.95	1.1	1.0434	1.0099
	36	0	100	100.00	54.841		69	0.95	1.1	1.0436	1.0280
	40	0	100	88.192	64.417		70	0.95	1.1	1.0184	1.0096
	42	0	100	83.016	49.460		72	0.95	1.1	1.0066	1.0062
	46	0	119	19.417	44.338		73	0.95	1.1	1.0092	1.0190
	49	0	304	138.66	140.370		74	0.95	1.1	1.0119	1.0264
	54	0	148	59.984	98.543		76	0.95	1.1	1.0045	1.0089
	55	0	100	74.764	52.457		77	0.95	1.1	1.0367	1.0170
	56	0	100	59.627	46.8259		80	0.95	1.1	1.0229	1.0183
	59	0	255	117.12	115.881		85	0.95	1.1	0.9985	1.0125
	61	0	260	121.66	121.893		87	0.95	1.1	0.9617	1.0290
	62	0	100	35.517	44.630		89	0.95	1.1	1.0269	1.0266
Power (MW)	65	0	491	214.33	213.346		90	0.95	1.1	1.0321	1.0253
	66	0	492	205.83	187.419		91	0.95	1.1	1.0209	1.0221
	70	0	100	12.582	54.0066		92	0.95	1.1	1.0237	1.0056
	72	0	100	12.141	40.751		99	0.95	1.1	1.0297	1.0222
	73	0	100	55.579	50.455		100	0.95	1.1	1.0412	1.0206
	74	0	100	14.137	42.021		103	0.95	1.1	1.0269	1.0326
	76	0	100	75.678	37.592		104	0.95	1.1	1.0484	1.0319
	77	0	100	82.194	42.539		105	0.95	1.1	1.0531	1.0203
	80	0	577	256.72	270.903		107	0.95	1.1	1.0380	1.0324
	85	0	100	42.579	42.382		110	0.95	1.1	1.0685	1.0243
	87	0	104	0.000	19.159		111	0.95	1.1	1.0854	1.0296
	89	0	707	257.13	216.783		112	0.95	1.1	1.0619	1.0349
	90	0	100	97.811	36.604		113	0.95	1.1	1.0228	1.0236
	91	0	100	8.436	52.187		116	0.95	1.1	1.0519	1.0073
	92	0	100	45.760	43.249		64	0.95	1.1	1.0160	1.0149
	99	0	100	23.885	40.178		65	0.95	1.1	1.0453	1.0229
	100	0	352	113.62	150.771		8	0.9	1.1	0.9897	1.0013
	103	0	140	42.612	50.598		32	0.9	1.1	1.0611	1.0167
	104	0	100	11.805	45.019		36	0.9	1.1	0.9508	0.9920
	105	0	100	100.00	63.106		51	0.9	1.1	1.0001	0.9742
	107	0	100	19.672	39.046	Tap ratio	93	0.9	1.1	0.9995	1.0096
	110	0	100	56.657	53.624		95	0.9	1.1	0.9000	1.0180
	111	0	136	22.867	43.765		102	0.9	1.1	1.0099	1.0270
	112	0	100	40.659	39.005		107	0.9	1.1	0.9262	0.9814
	113	0	100	16.067	51.229		127	0.9	1.1	0.9770	0.9995
	116	0	100	39.564	44.049		34	0	25	6.1168	14.2885
	64	0	100	99.998	74.484		44	0	25	14.0212	11.8200
	65	0	100	99.998	61.143		45	0	25	24.0656	12.7371
	1	0.95	1.1	1.0554	1.0093		46	0	25	9.5124	15.7212
	4	0.95	1.1	0.9500	1.0106		48	0	25	5.8489	14.8892
	6	0.95	1.1	0.9753	1.0256		74	0	25	19.2222	10.8066
	8	0.95	1.1	0.9585	1.0102	Shunt VAR compensator (MVAR)	79	0	25	0.0000	15.8930
	10	0.95	1.1	1.0381	1.0205		82	0	25	24.7411	13.8225
	12	0.95	1.1	1.0502	1.0141		83	0	25	13.9104	11.6974
Voltage (p.u.)	15	0.95	1.1	0.9529	1.0094		105	0	25	24.9944	13.5413
	18	0.95	1.1	0.9960	1.0220		107	0	25	19.0262	15.0743
	19	0.95	1.1	1.0077	1.0321		110	0	25	12.1782	11.1250
	24	0.95	1.1	0.9956	1.0184						
	25	0.95	1.1	1.0117	1.0251	TC ($/h)	-	-	-	**132958.66**	**135774.93**
	26	0.95	1.1	1.0397	1.0227	APL (MW)	-	-	-	**31.2916**	**39.6333**
	27	0.95	1.1	1.0466	1.0121	VMD (p.u)	-	-	-	-	**0.4299**

Table 8: IEEE 118-bus systems: comparison of the proposed method with MOEA/D [33], NSGA-II [34], and MOPSO [35] for Case-9 to Case-10.

Case name	Objective functions	Proposed method	MOEA/D [33]	NSGA-II [34]	MOPSO [35]
Case-9	TC ($/h)	**132958.66**	133249.84	133837.90	134673.5
	APL (MW)	**31.2916**	31.8104	31.8664	35.3868
Case-10	TC ($/h)	**135774.93**	135801.21	135912.8	136459.9
	APL (MW)	**39.6333**	42.0412	45.6904	48.3446
	VMD (p.u.)	**0.4299**	0.4523	0.5074	0.5878

could be found using the proposed algorithm have a TC of **36207.21$/h**, a TE of **1.0916ton/h,** APL of **9.9732 MW**, and VMD of **0.6848p.u.,** which is the lowest value compared with MOEA/D [33], NSGA-II [34], and MOPSO [35] as shown in Table 6.

5.3. Modified IEEE 118-Bus System. To show the scalability of the proposed algorithm for a large-scale test system in solving the MOOPF problem, the IEEE 118-bus system is considered. It contains 54 thermal generators (# 69 generator as a slack generator) and 186 lines. In this study, 9 off-nominal transformers and 12 shunt VAR compensators are considered. The sum of real and reactive power demand on the system is 4242.00 MW and 1439.00MVAR, respectively. In addition to the above thermal generators, one wind generator and one solar unit are added to buses 63 and 64, respectively. Detailed information about the test system is provided in [39, 40].

5.3.1. Case-9: Simultaneously Minimize TC and APL. In this case, TC and APL are the objectives that need to be simultaneously minimized. The optimal decision variables obtained by the suggested method are included in Table 7. The best compromise solution that could be found using the proposed algorithm has a TC of **132958.66$/h** and an APL of **31.2916 MW,** which is the lowest value compared with MOEA/D [33], NSGA-II [34], and MOPSO [35] as shown in Table 8. The Pareto optimal fronts of all the methods are depicted in Figure 7.

5.3.2. Case-10: Simultaneously Minimize TC, APL, and VMD. In this case, TC, APL, and VMD are the objectives that need simultaneous minimizing. The optimal decision variables obtained by the suggested method are included in Table 7. The best compromise solution that could be obtained using the proposed algorithm has a total cost of **135774.93$/h**, APL of **39.6333 MW**, and VMD of **0.4299p.u.**, which is the lowest value compared to MOEA/D [33], NSGA-II [34], and MOPSO [35] as shown in Table 8. The Pareto optimal fronts of all the methods are depicted in Figure 8.

5.4. Computational Time. In this study, the MOOPF problem was executed on a 2.00 GHz, i3 processor, with a 4 GB RAM computer. The computational (CPU) times of the proposed method, MOEA/D, NSGA-II, and MOPSO for all the cases are given in Table 9. The computational times of the proposed method are significantly faster than those of other studied methods for all cases. Hence, the proposed method outperformed the other methods in terms of solution quality and computing time.

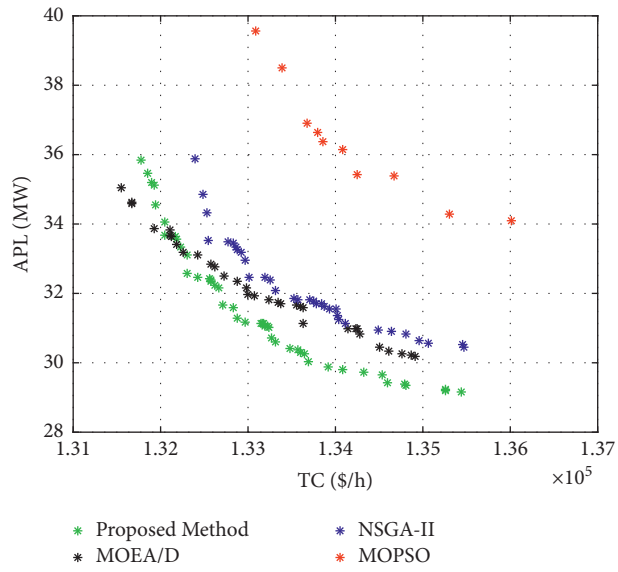

Figure 7: Case-9: IEEE 118-bus system Pareto optimal fronts.

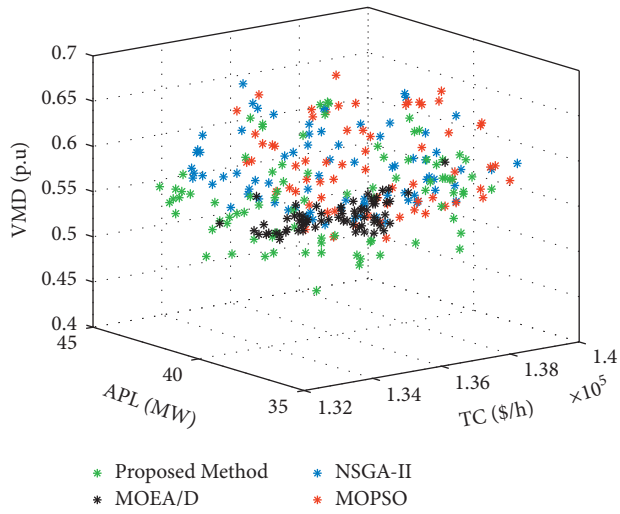

Figure 8: Case-10: IEEE 118-bus system Pareto optimal fronts.

Table 9: Comparison of CPU time (sec).

	Case name	Proposed method	MOEA/D [33]	NSGA-II [34]	MOPSO [35]
IEEE 30-bus system	Case-1	**845.19**	1333.57	1615.12	1014.31
	Case-2	**853.92**	1413.40	1460.24	1029.56
	Case-3	**856.94**	1342.81	1700.27	1198.45
	Case-4	**915.49**	1351.51	1500.08	1201.34
	Case-5	**1009.63**	1372.80	1750.88	1279.83
IEEE 57-bus system	Case-6	**1105.04**	1672.55	1967.01	1401.21
	Case-7	**1146.21**	1709.16	2046.42	1456.89
	Case-8	**1190.14**	1887.68	2054.09	1523.47
IEEE 118-bus system	Case-9	**1535.33**	2771.16	2946.30	1881.56
	Case-10	**1705.10**	2833.67	3219.41	2015.64

6. Conclusions

This study proposes a solution to the MOOPF problem with a combination of thermal, wind, and PV systems using MOEA based on decomposition and summation of normalized objectives with an improved diversified selection method. The method also deals with tackling various constraints in the MOOPF problem using the superiority of the feasible solution (SF) technique. The fuel costs of thermal generators and uncertainty prices associated with wind and PV energy systems are minimized along with carbon emission, active power losses, and voltage magnitude deviation. Monte Carlo simulations were used to assess the uncertainty of wind and solar power. Apart from the conventional cost minimization, this study selects factors to account for the uncertain price of available wind and solar power. It depicts the OPF formulation along with factors affecting wind and PV power's intermittency. To show the efficacy of the suggested method, simulations were performed on the same test systems as with MOEA/D, NSGA-II, and MOPSO algorithms. The results show the superiority of the proposed method compared to other methods. Hence, the proposed method can be effectively used in operation and control when wind and solar power generation are included in the power system.

Abbreviations

k, c: Shape and scale factors, respectively
v: Wind speed (m/sec)
v_{in}, v_{out}, v_r: Cut-in, cut-out, and rated wind speeds, respectively
G_s: Solar irradiance
μ: Mean
σ: Standard deviation
P_{wr}, P_{sr}: Rated power of wind and solar plants, respectively
P_{ws}, P_{ss}: Scheduled power of wind and solar plants, respectively
g_j, h_k: Direct price coefficients of j^{th} a windmill and k^{th} solar plant, respectively
$P_{wav,j}$, $P_{sav,k}$: The actual power output of j^{th} windmill and k^{th} PV plant, respectively
$K_{Rw,j}$, $K_{Pw,j}$: Reserve and penalty price coefficients of j^{th} windmill, respectively
$K_{Rs,k}$, $K_{Ps,k}$: Reserve and penalty price coefficients of k^{th} PV plant, respectively
a_i, b_i, c_i: i^{th} Generator cost coefficients
N_{TG}, N_{WG}, and N_{SG}: Number of thermal, wind, and solar power plants, respectively
$\alpha_i, \beta_i, \gamma_i, \xi_i, \lambda_i$: i^{th} generator emission coefficients
G_{ij}, B_{ij}: Conductance and susceptance between buses i and j
N_B, N_{TG}, N_C, N_{PQ}, and N_T: Number of buses, thermal generators, shunt VAR compensators, PQ buses, and transformers, respectively
$P_{Gi}^{\min}$, $P_{Gi}^{\max}$: Min-max limits on i^{th} generator real power
$Q_{Gi}^{\min}$, $Q_{Gi}^{\max}$: Min-max limits on i^{th} generator reactive power
$S, S^{\max}$: Apparent power flow and its maximum limit, respectively
$T_k^{\min}$, $T_k^{\max}$: Min-max limits of k^{th} transformer tap positions
$V_i^{\min}$, $V_i^{\max}$: Min-max limits of i^{th} bus voltages
θ_{ij}: Voltage angle between buses i and j
P_{G_i}, Q_{G_i}: Real and reactive power injection at i^{th} bus
P_{D_i}, Q_{D_i}: Real and reactive power demand at i^{th} bus
w: Weight vector
n_l: Number of lines
M: Number of objectives
f'_m: Normalized m^{th} objective
MOEA: Multiobjective evolutionary algorithm
MOOPF: Multiobjective optimal power flow
PV: Photovoltaic
WT: Wind turbine
ISO: Independent system operator
NSGA-II: Nondominated sorting genetic algorithm-II
MOPSO: Multiobjective particle swarm optimization.

Data Availability

The data supporting these findings are from previously reported studies and datasets, which have been cited.

Conflicts of Interest

The authors declare that they have no conflicts of interest.

References

[1] C. Haiyan, C. Jinfu, and D. Xian Zhong, "Multi-stage dynamic optimal power flow in wind power integrated system," in *Proceedings of the IEEE/PES Transmission and Distribution Conference and Exhibition: Asia and Pacific*, pp. 1–5, Dalian, China, June 2005.

[2] A. Domingos and M. P. M. Pedro, *Optimal Power Flow Including Wind Generation*, Instituto Superior Tecnico, Technical University of Lisbon, Lisbon, Portugal, 2012.

[3] P. P. Biswas, P. N. Suganthan, and G. A. J. Amaratunga, "Optimal power flow solutions incorporating stochastic wind and solar power," *Energy Conversion and Management*, vol. 148, pp. 1194–1207, 2017.

[4] M. H. Sulaiman, Z. Mustaffa, A. J. Mohamad, M. M. Saari, and M. R. Mohamed, "Optimal power flow with stochastic solar power using barnacles mating optimizer," *Int. Trans. Electr. Energy Syst.,* vol. 66, pp. 88–93, 2021.

[5] C. Mishra, S. P. Singh, and J. Rokadia, "Optimal power flow in the presence of wind power using modified cuckoo search," *IET Generation, Transmission & Distribution*, vol. 9, no. 7, pp. 615–626, 2015.

[6] K. Teeparthi and D. M. Vinod Kumar, "Security-constrained optimal power flow with wind and thermal power generation using fuzzy adaptive artificial physics optimization algorithm," *Neural Computing & Applications*, vol. 29, no. 3, pp. 855–871, 2016.

[7] H. T. J. Ranjit Roy, "Optimal power flow solution of power system incorporating stochastic wind power using Gbest guided artificial bee colony algorithm," *International Journal of Electrical Power & Energy Systems*, vol. 64, pp. 562–578, 2015.

[8] S. Duman, J. Li, and L. Wu, "AC optimal power flow with thermal-wind-solar-tidal systems using the symbiotic organisms search algorithm," *IET Renewable Power Generation*, vol. 15, pp. 278–296, 2021.

[9] E. E. Elattar and S. K. Elsayed, "Modified JAYA algorithm for optimal power flow incorporating renewable energy sources considering the cost, emission, power loss and voltage profile improvement," *Energy*, vol. 178, pp. 598–609, 2019.

[10] Z. Ullah, S. Wang, J. Radosavljevic, and J. Lai, "A solution to the optimal power flow problem considering WT and PV generation," *IEEE Access*, vol. 7, pp. 46763–46772, 2019.

[11] P. K. Roy and C. Paul, "Optimal power flow using krill herd algorithm," *Int. Trans. Electr. Energy Syst.,* vol. 25, 2014.

[12] M. A. Taher, S. Kamel, F. Jurado, and E. Mohamed, "An improved moth-flame optimization algorithm for solving optimal power flow problem," *Int. Trans. Electr. Energy Syst.,* vol. 29, 2018.

[13] A. Saha, A. Bhattacharya, P. Das, and A. K. Chakraborty, "A novel approach towards uncertainty modeling in multi-objective optimal power flow with renewable integration," *Int. Trans. Elect. Energy Syst.,* vol. 29, no. 12, p. 12136, 2019.

[14] S. Duman, S. Rivera, J. Li, and L. Wu, "Optimal power flow of power systems with controllable wind-photovoltaic energy systems via differential evolutionary particle swarm optimization," *Int. Trans. Elect. Energy Syst.,* vol. 30, no. 4, p. 12270, 2020.

[15] S. Duman, J. Li, L. Wu, and U. Guvenc, "Optimal power flow with stochastic wind power and FACTS devices: a modified hybrid PSOGSA with chaotic maps approach," *Neural Computing & Applications*, vol. 32, pp. 8463–8492, 2019.

[16] S. R. Salkuti, V. Sandeep, B. C. babu, and C.-M. Jung, "Multi-objective based optimal generation scheduling considering wind and solar energy systems," *International Journal of Emerging Electric Power Systems*, vol. 19, no. 5, Article ID 20180006, 2018.

[17] K. Deb, *Optimization for Engineering Design: Algorithms and Examples*, Prentice-Hall, New Delhi, India, 1995.

[18] G. V. Reklaitis, A. Ravindran, and K. M. Ragsdell, *Engineering Optimization Methods and applications*, Wiley, New York, NY, USA, 1983.

[19] C. Chun-Lung, T. Y. Lee, and R. M. Jan, "Optimal wind-thermal coordination dispatch in isolated power systems with large integration of wind capacity," *Energy Conversion and Management*, vol. 47, pp. 3456–3472, 2006.

[20] J. Hetzer, D. C. Yu, and K. Bhattarai, "An economic dispatch model incorporating wind power," *IEEE Transactions on Energy Conversion*, vol. 23, no. 2, pp. 603–611, 2008.

[21] T. P. Chang, "Investigation on frequency distribution of global radiation using different probability density functions," *Int. J. of Appl. Science and Engg.,* vol. 8, no. 2, pp. 99–107, 2010.

[22] S. S. Reddy, P. R. Bijwe, and A. R. Abhyankar, "Real-time economic dispatch considering renewable power generation variability and uncertainty over scheduling period," *IEEE Systems Journal*, vol. 9, no. 4, pp. 1440–1451, 2015.

[23] A. Panda and M. Tripathy, "Security constrained optimal power flow solution of wind-thermal generation system using bacterial foraging algorithm," *Energy*, vol. 93, pp. 816–827, 2015.

[24] L. Shi, C. Wang, L. Yao, Y. Ni, and M. Bazargan, "Optimal power flow solution incorporating wind power," *IEEE Systems Journal*, vol. 6, no. 2, pp. 233–241, 2012.

[25] O. Aslac and B. Stott, "Optimal load flow with steady-state security," *IEEE Transactions on Power Apparatus and Systems*, vol. 3, pp. 745–751, 1974.

[26] R. D. Zimmerman, C. E. Murillo-Sanchez, and R. J. Thomas, "MATPOWER," http://www.pserc.cornell.edu/matpower.

[27] T. Ackermann, *Wind Power in Power System*, John Wiley & Sons, New York, NY, USA, Chapter 43, 2012.

[28] S. Eftekharnejad, V. Vittal, G. T. Heydt, B. Keel, and J. Loehr, "Impact of increased penetration of photovoltaic generation on power systems," *IEEE Transactions on Power Systems*, vol. 28, no. 2, pp. 893–901, 2013.

[29] K. Deb, "An efficient constraint handling method for genetic algorithms," *Computer Methods in Applied Mechanics and Engineering*, vol. 186, pp. 311–338, 2000.

[30] K. Li, K. Deb, Q. Zhang, and S. Kwong, "An evolutionary many-objective optimization algorithm based on dominance and decomposition," *IEEE Transactions on Evolutionary Computation*, vol. 19, no. 5, pp. 694–716, 2015.

[31] Q. Zhang and H. Li, "MOEA/D: a multi objective evolutionary algorithm based on decomposition," *IEEE Transactions on Evolutionary Computation*, vol. 11, no. 6, pp. 712–731, 2007.

[32] B. Y. Qu and P. N. Suganthan, "Multi-objective differential evolution based on the summation of normalized objectives and improved selection method," in *Proceedings of the IEEE Symposium*, pp. 1–8, Anchorage, AL, USA, May 2011.

[33] J. Zhang, Q. Tang, P. Li, D. Deng, and Y. Chen, "A modified MOEA/D approach to the solution of multi-objective optimal power flow problem," *Applied Soft Computing*, vol. 47, pp. 494–514, 2016.

[34] K. Deb, A. Pratap, S. Agarwal, and T. Meyarivan, "A fast and elitist multi objective genetic algorithm: NSGA-II," *IEEE Transactions on Evolutionary Computation*, vol. 6, no. 2, pp. 182–197, 2002.

[35] C. Coello, G. T. Pulido, and M. S. Lechuga, "Handling multiple objectives with particle swarm optimization," *IEEE Transactions on Evolutionary Computation*, vol. 8, no. 3, pp. 256–279, 2004.

[36] I. Das and J. E. Dennis, "Normal –boundary intersection: a new method for generating Pareto optimal points in multicriteria optimization problems," *SIAM Journal on Optimization*, vol. 8, no. 3, pp. 631–657, 1998.

[37] Y. Zhang and Y. Li, "A many-objective evolutionary algorithm based on decomposition and local dominance," 2018.

[38] M. A. Abido, "Environmental/economic power dispatch using multi-objective evolutionary algorithms: a comparative study," *IEEE Transactions on Power Systems*, vol. 1, no. 4, pp. 1529–1537, 2003.

[39] A. Shabanpour-Haghighi, A. R. Seifi, and T. Niknam, "A modified teaching-learning based Optimization for multi-objective optimal power Flow problem," *Energy Conversion and Management*, vol. 77, pp. 597–607, 2014.

[40] R. D. Zimmerman, C. E. Murillo-Sanchez, and R. J. Thomas, "MATPOWER: steady-state operations, planning, and analysis tools for power systems research and education," *IEEE Transactions on Power Systems*, vol. 26, pp. 9–12, 2011.